JOM, Vol. 74, No. 6, 2022
https://doi.org/10.1007/s11837-022-05278-0

Nanoindentation for Fast Investigation of PET Film Degradation

PETRA CHRISTÖFL ,[1,4,5] BETTINA OTTERSBÖCK,[1] CATERINA CZIBULA,[2] ASTRID MACHER,[1] CHRISTIAN TEICHERT,[3] GERALD PINTER,[4] and GERNOT ORESKI[1]

1.—Polymer Competence Center Leoben, Leoben, Austria. 2.—Institute of Bioproducts and Paper Technology, Graz University of Technology, Graz, Austria. 3.—Insitute of Physics, Montanuniversität Leoben, Leoben, Austria. 4.—Materials Science and Testing of Polymers, Montanuniversität Leoben, Leoben, Austria. 5.—e-mail: petra.christoefl@pccl.at

The lifetime of industrial polymer products is in many cases limited by aging. Therefore, it is necessary to develop a fast and sensitive method to detect polymer aging at an early stage. A commercially available 50-μm-thick and transparent polyethylene terephtalate (PET) film was aged under different artificial conditions, and the evolution of mechanical properties with increasing aging time was investigated via nanoindentation (NI) and tensile testing. Chemical aging was studied with gel permeation chromatography (GPC), and physical aging was monitored by the first heating of differential scanning calorimetry. NI data evaluated with the method of Oliver and Pharr was compared to tensile test data with good agreement between the results on the macro- and nanoscales. Furthermore, a correlation between NI creep data and GPC data was obtained, which indicates that the aging of the PET films primarily originated from chemical aging. This study states that NI is an appropriate method to determine degradation of PET at an early stage.

INTRODUCTION

Polymers like polyethylene terephtalate (PET) are used in different fields of industry ranging from applications in the packaging[1] and fiber sectors[2] to the utilization as backsheets in photovoltaic modules.[3,4] One big issue of polymers applied in demanding applications is degradation, especially when they are exposed over time to elevated temperatures and humidity. The sum of all the physical and chemical changes of a polymer during application time is defined as aging. To make polymers more sustainable and reliable regarding their area of application, it is essential to understand their mechanical behaviour before and after the degradation processes. Nanoindentation (NI), a standard depth-sensing technique for testing the local mechanical properties of materials, holds a good possibility to investigate aged polymers. The Oliver and Pharr (O&P)[5] method was established to identify mechanical properties from NI tests. It was primarily developed for linear elastic, hard, and isotropic materials, based on the theory of Hertz,[6] with frictionless surfaces in non-conforming contact.[7] Although mostly applied to metals, NI studies for polymers have been gaining interest in recent times.[8–11] Yet, it needs to be considered that polymers are—in contrast to metals—viscoelastic materials which exhibit a time-dependent mechanical behavior. Therefore, several limitations need to be considered when applying the O&P method to polymers.[12–14]

PET is a commonly used thermoplastic polymer,[15] which is known to hydrolyse above its glass transition temperature,[16] leading to significantly shorter molecular chains and lower molecular mass.[15] In addition to this irreversible chemical aging due to hydrolysis, PET also shows reversible physical aging in terms of the reorientation and recrystallization of the molecular fragments.[17] There have been reports on the influence of aging on the mechanical properties of semi-crystalline PET.[17–21] However, to the authors' knowledge, there is no study on the correlation of bulk- and nanomechanical properties with the chemical aging effects of PET under aging conditions.

(Received December 31, 2021; accepted March 21, 2022; published online April 20, 2022)

The main goal of this work is to demonstrate that NI is capable of determining the mechanical properties of aged PET by analyzing the change of the elastic modulus, similar to a tensile test. The aging effect is further demonstrated by comparison with an unaged PET sample. Furthermore, it will be pointed out that, with the method of NI, the elastic modulus of severely degraded (embrittled) materials can also be distinguished, which is hardly possible with tensile testing due to the impeded sample preparation. A further important goal is to prove that NI in the creep mode correlates with the loss in molecular weight of PET, and therefore to chemical aging. This NI creep method is presented as a quick and sensitive method to detect the degradation of PET, as well as mechanical changes of PET at an early stage of aging.

MATERIALS AND METHODS

PET Samples

For the following study, a commercially available 50-μm-thick and transparent PET film was investigated. The film was manufactured by co-extrusion, where it was biaxially drawn in a 3-layer construction. These films are widely used as a component in backsheets for photovoltaic (PV) modules; further details about the PET samples are provided in Ref. 22. Seven batches of PET were chosen for our investigations. The aging of each of the batches with sample numbers 1–6 was performed, according to the scheme in Table I, in the climate chamber WLK 64-40 (Weiss Umwelttechnik, Vienna, Austria) with 85% RH. An unaged PET sample served as a reference (sample number 7).

For NI, each sample (as presented in Table I) was cut into a 50 μm × 1.5 cm × 1 cm piece which had been embedded separately in epoxy resin. Then, they were ground with silicon carbide up to a grain size of 4000, and polished with 3-μm and 1-μm diamond polishing paste.

NI tests were performed on the polished surface of each sample according to the measurement scheme in Fig. 1. For each sample, 20 measurements were performed in the position "edge", and 20 measurements were performed in the position "middle" for the O&P measuring approach (see "Nanoindentation Oliver & Pharr" section). Furthermore, 20 measurements were performed in the position "edge" and 20 measurements were performed in the position "middle" for the nanoindentation creep mode (see "Nanoindentation Creep" section). For the tensile tests, rectangular samples with a size of 15 mm × 100 mm were cut out.

Nanoindentation Oliver & Pharr

Nanoindentation curves were evaluated by the O&P method.[5] The fitting of the unloading curve of the indentation load penetration curve was executed by Eq. 1:

$$\frac{F}{F_{\max}} = \left(\frac{h - h_p}{h_{\max} - h_p}\right)^m \tag{1}$$

Here, $h_{\max}$ is the contact depth of the indenter at the maximum force $F_{\max}$, h_p is the permanent indentation depth, and m is the fitting parameter.[23] The slope of the fit $S = \left(\frac{dF}{dh}\right)_{\max}$ is the contact stiffness for the upper portion of the unloading curve. The contact area of the indenter tip for $h_{\max}$ is $A_p = f(h_{\max})$. The reduced modulus, E_r, is calculated by Eq. 2:[23]

$$E_r = \frac{\pi S}{2\beta\sqrt{A_p(h_{\max})}} \tag{2}$$

E_r is thereby obtained assuming that the unloading is purely elastic. The geometry factor, β, equals 1 for a circular sphero-conical indenter tip. The contact area at maximum load $A_p = f(h_{\max})$ is determined by the depth of the contact and the indenter tip geometry.[5]

For calibration, the functional form of $f(h)$ was computed on a fused silica reference sample from Anton Paar, with a thermal drift < 0.2 pm/s.[24] Equation 3 defines the relationship between E_i the elastic modulus of the indenter ($E_{\text{diamond}} = 1141$ GPa), the elastic modulus E, and the reduced modulus E_r:

$$\frac{1}{E_r} = \frac{(1 - \nu^2)}{E} + \frac{(1 - \nu_i^2)}{E_i} \tag{3}$$

ν_i is the Poisson's ratio of the indenter tip with $\nu_{\text{diamond}} = 0.07$. For the following experiments, we defined $\nu = 0.3$ for PET.[25] Further details about the applied method can be found in our previous works.[8,9]

For the current study, an Anton Paar UNHT^3 Nanoindenter (Anton Paar, Graz, Austria) was employed. For practical reasons, the fit of the unloading curve was performed between 75% and 95% of $F_{\max}$. Tests were performed using an Anton Paar diamond sphero-conical nanoindenter tip (SD-C06), with a tip radius of 10 μm and an opening angle of 90°. NI tests were performed on the embedded PET samples under the laboratory conditions of 22°C temperature and 30% RH in a matrix according to Fig. 1, with a distance of 20 μm between each indent in the x direction at two positions in the middle and on the edge of the sample. The loading and unloading ramps during the experiment were performed linearly with a load rate of 30 mN/min and a maximum load of 15 mN. The holding phase at constant force was 30 s. The software "Indentation 8.0.24" (Anton Paar) was employed for recording and evaluation of the data. The elastic modulus was calculated from 20 measurements for each position, and the results are given in terms of mean ± standard deviation.

Table I. Climate chamber aging parameters of the PET samples at a relative humidity of 85%

Sample number	Aging time (h)	Aging temperature (°C)
1	1000	85
2	2000	85
3	3000	85
4	1000	95
5	2000	95
6	3000	95
7	Unaged	

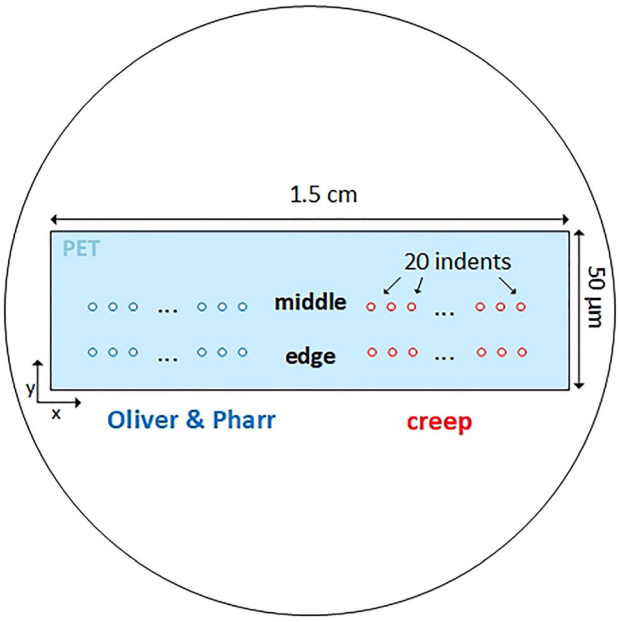

Fig 1. The embedded cross-section of PET samples with exemplary indents marked as coloured circles: Oliver & Pharr approach (blue) and creep measurement (red) each in the positions middle and edge (Color figure online).

Nanoindentation Creep

NI creep tests were performed with the spheroconical indenter under laboratory conditions of 22°C temperature and 30% relative humidity (RH), according to Fig. 1. The distance between each indent in the x direction was 20 μm for each position in the middle and on the edge of the sample. The loading of the samples was performed linearly with a 250-mN/min load rate up to a maximum load of 15 mN. The holding phase at constant force was 300 s, when the creep of the PET samples was recorded. To compare the creep behavior of differently aged PET samples, mean creep curves from 20 measurements for the positions middle and edge were calculated and normalized.

Tensile Tests

Tensile tests were carried out with a Zwick Roell Z001 testing device (Ulm, Germany) at ambient conditions according to EN ISO 527-3,[26] with a testing speed of 50 mm/min and a gauge length of 50 mm. The elastic modulus was determined for at least 7 samples per test series.

Gel Permeation Chromatography (GPC)

An Agilent Technologies GPC 50 (Santa Clara, USA) device with two detectors (one recording the refractive index and a 4-capillar viscosity detector) was used along with two PSS SDV analytical linear M columns (8 × 50 mm and 8 × 300 mm) having a particle size of 5 μm. A universal calibration with polystyrol (PS) (K = 1.91 10^{-4} dl g^{-1} and α = 0.693) and a detector calibration with PS standard 133,000 Da was carried out to provide proper calculation of the molecular weight.[27] The samples were dissolved in pure hexafluoroisopropanol (HFIP), with subsequent slow dilution with chloroform ($CHCl_3$) to reach a final concentration of around 2.5 mg ml^{-1} in a $CHCl_3$:HFIP mixture (98:2 vol%). A stable temperature of 40°C at the beginning of the experiment was chosen in order to prevent early precipitation of the samples. The amount of the injected sample was 100 μl.

Differential Scanning Calorimetry (DSC)

DSC was performed with a Perkin Elmer DSC 4000 (Waltham, USA) to determine the thermal behaviour of PET in the range of 23–270°C with a heating rate of 10 K min^{-1}. About 10 mg of the samples were cut and put into 50-μl pans with perforated lids. To prevent a further oxidation process, the measurements were performed in a nitrogen atmosphere. Peak temperatures and enthalpies for melting and crystallization were evaluated according to ISO 11357-3,[28] with three samples to obtain an average.

RESULTS AND DISCUSSION

Aging-Induced Molecular Changes

The main mechanisms in polymer aging studied within this report are physical (reversible) and chemical (irreversible). Physical aging processes effect changes in physical properties with the main phenomena of relaxation and post-crystallization. Chemical aging affects the chemical composition and molecular structure and the weight of a

polymer.[29] The influence of chemical aging on the entire aging process can be observed by measuring the molecular weight by GPC. Figure 2a shows the evolution of molecular mass with aging time gained by GPC measurements for the temperatures 85°C and 95°C, both with 85% RH.

The molecular mass decreases from approximately 26,300 g mol^{-1} to values below 10,000 g mol^{-1} for samples aged at 85°C as well as at 95°C. The decrease is more dominant for the 95°C aged samples. Humidity and elevated temperature lead to chemical aging of PET by hydrolysis. Here, chain scission takes place at ester linkages where water molecules break down ester bonds. Such reverse esterification leads to smaller chain fragments of the main chains of PET, and therefore to a decline of molecular weight.[30,31]

Physical aging is a reversible and temperature-induced process and can be observed in the first heating curve of DSC. Figure 2b shows DSC curves for the first heating of PET aged at 85% RH for 0 h, 1000 h, 2000 h, and 3000 h at 85°C and 95°C. The first DSC heating of the samples aged at 85°C shows no significant differences in crystalline structures, as indicated by Fig. 2b. For samples aged at 95°C, slight changes of the melting peak with further aging time were detected. An alteration of the peak shape for 95°C-aged PET samples indicates that the crystal heterogeneity was increased during degradation, which leads to slight recrystallization and reorientation processes of the molecular chains.[32] In addition, there was no sign of physical aging. Looking at Fig. 2, chemical aging does not seem to be the only triggering factor for physical aging. The glass transition of the unaged PET is in the range of 70–115°C with the peak temperature at 106°C, whereas for aged PET (85°C, 85% RH and 95°C, 85% RH) the glass transition temperature peak (Tg) is above 110°C.[22] Aging at temperatures in the range of its glass transition provides physical aging,[33] and leads to recrystallization and reorientation, as seen in the first heating of DSC. Samples aged at 95°C are more affected by this process than the 85°C-aged samples, because of the proximity to Tg.

Evolution of the Elastic Modulus from PET Aging

There is evidence in the literature that the aging of PET influences its mechanical properties.[17,29,34,35] Figure 3 shows the elastic modulus depending on aging time of the PET samples gained by the NI O&P method, as well as the tensile testing results for the aging conditions 85°C (Fig. 3a) and 95°C (Fig. 3b) accompanied by the results of the unaged samples.

Moduli from the tensile tests match the NI results quite well, except for the samples aged for 3000 h at 85°C, where the samples were strongly embrittled. Fractures of the tensile test specimens during the tensile tests start at a defect which acts as a notch. Compared to low embrittled (unaged) material, sample preparation on highly embrittled material is likely to cause more defects in the test specimens, which disproportionately influences the tensile test results. Samples from 2000 h and 3000 h with 95°C aging were too brittle for tensile testing, and therefore those samples were investigated only by NI (see Fig. 3b).

Although there is a slight trend towards higher elastic moduli with higher aging time for 85°C (Fig. 3a), the modulus determined by both methods does not change significantly. However, for PET samples aged at 95°C (Fig. 3b), the elastic modulus obtained by both methods increases significantly. As already observed in Fig. 2a, aging leads to a reduction of molecular weight caused by chain scission. This is followed by a decrease of the macromolecule concentration and interlamellar spacing, both leading to embrittlement and an increasing elastic modulus of PET with aging.[29,34] The molecular mass reduction is more pronounced for samples degraded at 95°C, hence the aging effect is also more visible in terms of elastic modulus. Furthermore, previous investigations detected a rising elastic modulus gained by the NI O&P method from degradation,[36,37] which is in good accordance with the findings of this work.

The difference in the elastic moduli of NI in the positions middle and edge of the unaged sample is remarkable, which may be caused by the semi-crystalline structure of PET. In a previous publication,[9] we have shown that semi-crystalline polyoxymethylene (POM) exhibits a layered morphological structure leading to different elastic moduli for the middle and edge of the cross-sectional sample. Investigations of a cross-sectional tensile bar of injection-molded POM by NI revealed that a less semi-crystalline skin layer, originating from the production process, leads to lower elastic moduli, whereas the more semi-crystalline core layer leads to significantly higher elastic moduli.[9] As for POM, PET also shows a lower modulus at the edge of the sample and a higher modulus in the middle (Fig. 3). Also[38] discovered, from indentation experiments on PET foils, that amorphous layers of PET show lower elastic moduli in contrast to crystalline layers with higher elastic moduli.

Nevertheless, the embedding material (epoxy resin) also influences the NI results at the edge of the sample. Since the indentation depth is about 1–2 μm, as presented in Figure S1 in the Supplementary Material, the stress field of indentation is rather small. The influence of the embedding material on the NI results of the PET samples is assumed to be minor. For quantitative analysis of the elastic modulus over aging time, the influence of the embedding material stays the same for all the sample and is therefore neglectable.

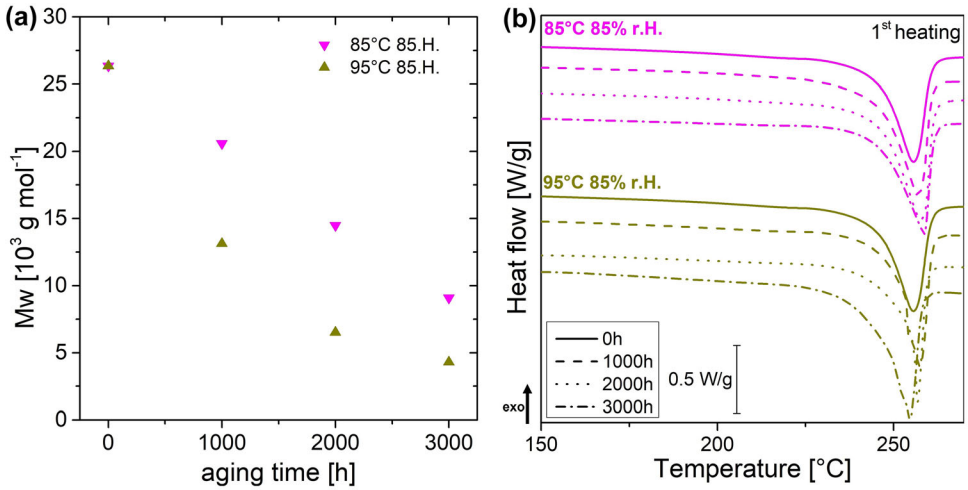

Fig 2. (a) Molecular weight over aging time for 85°C at 85% RH and 95°C at 85% RH, and (b) DSC curves for the first heating of PET aged for 0 h, 1000 h, 2000 h, and 3000 h with conditions of 85°C at 85% RH and 95°C at 85% RH.

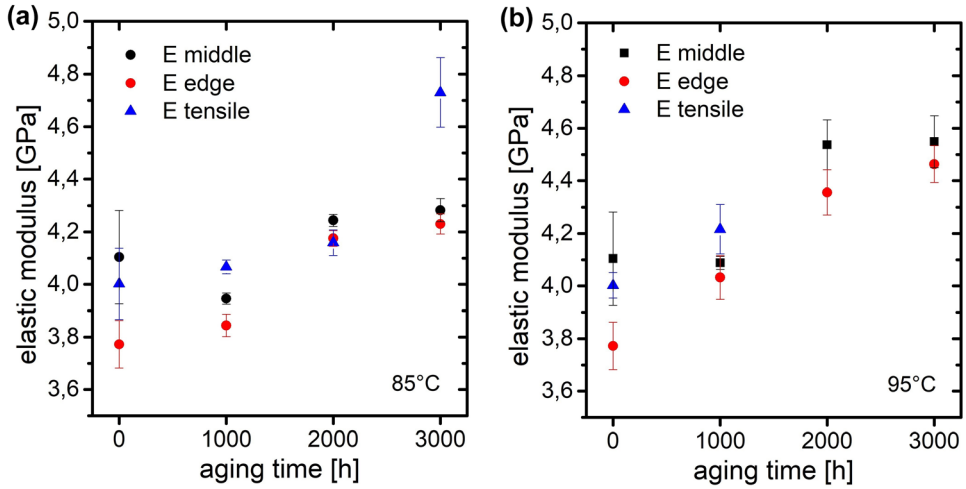

Fig 3. Development of the elastic modulus from NI (black dots-middle, red dots-edge) and tensile test (blue triangles) over aging time with 85°C and 85% RH (a), and 95°C and 85% RH (b). The elastic modulus was calculated in terms of mean and standard deviation (Color figure online).

NI Creep in Context to Molecular Weight

Representative data of creep curves obtained by NI are presented in Fig. 4 for each aging condition and position, where the normalized indentation depth correlates with the aging time. The unaged sample exhibits the highest creep, followed by samples aged at 85°C with ascending aging times from 1000 h to 3000 h. Samples aged with 3000-h aging time indicate the lowest creep. The same trend was recognized for samples aged at 95°C. Such a decrease in the creep behavior with increasing aging time for PET was also observed for NI studies.[39]

When comparing NI creep at the positions at the middle and edge of the sample, it should be noticed that PET reveals more creep at the edge for the unaged sample. The reason for this may originate from the layered structure of semi-crystalline PET, with more amorphous phases at the edge of the sample and more crystalline phases in the center. A detailed investigation of this behavior has been published in Ref. 9 for POM. For longer aging times, the difference between the middle and the edge decreases by means of the creep behavior. The DSC results indicate minor recrystallization processes for the aged samples, which may lead to a more homogenized morphology throughout the sample, and a more homogeneous creep behavior in the middle and edge of the samples.

The maximum of the normalized indentation depth (from Fig. 4) correlates clearly with the molecular weight (M_w), which is depicted in Fig. 5. Here, the results for the M_W obtained from the GPC measurements, which are presented in Fig. 2a, are plotted logarithmically. For PET samples aged with 85°C (Fig. 5a), the logarithmic correlation between the molecular weight and the indentation depth follows a polynomial fit for the position middle (R = 0.99) and a linear fit (R= 0.90) for the position

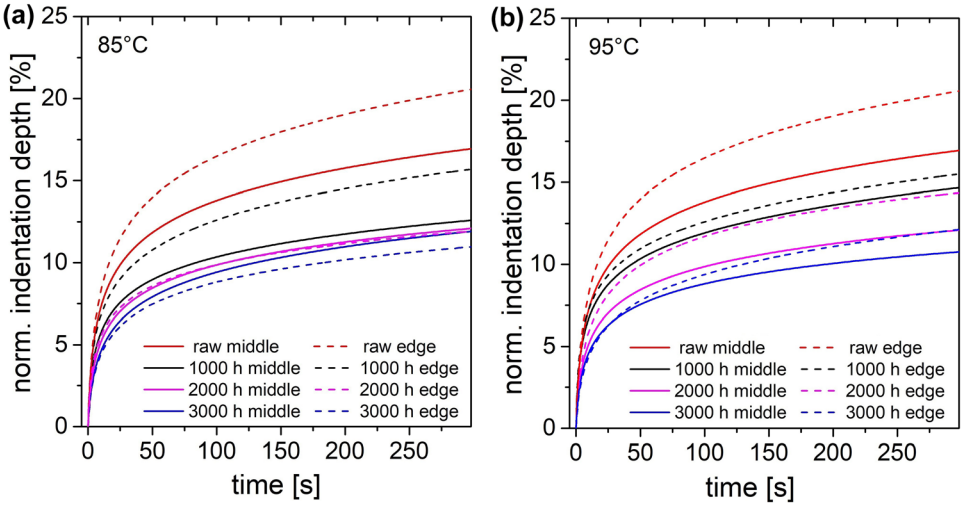

Fig 4. Normalized mean creep curves obtained from 20 individual curves for different aging (0 h, 1000 h, 2000 h, 3000 h) at (a) 85°C and 85% RH, and (b) 95°C and 85% RH. The positions middle and edge of the indents are indicated with a solid and dashed line, respectively.

edge. The logarithmic correlation in the position middle (R = 0.99) and edge (R = 0.98) between the maximum normalized indentation depth and the molecular weight of the PET samples aged with 95°C is linear (Fig. 5b).

The influence of molecular weight on NI creep compliance has previously been extensively investigated.[40] That work revealed that increasing molecular weight makes a polymer more creep-resistant. This observation was made, e.g., for injection-molded semi-crystalline polyethylene and polypropylene. It was stated that the application of a constant load during creep experiments results in intramolecular tensions. To decrease these tensions, a polymer with a high M_W can push low-strained molecule parts to highly-strained regions of the contact zone, and vice versa. This way, strains can be well distributed due to the high structural connectivity.

Here, this model is applied to unaged PET with its higher molecular weight in contrast to the lower molecular weight-aged PET. For unaged PET, the higher molecular weight with longer main chains exhibits higher connectivity between the high- and low-strain zones, which decreases the resistance to further indenter penetration and enlarges the creep. Regions with higher intramolecular tensions cause continued molecular displacement to reduce internal strain. Regarding aged PET, chain scission leads to shorter chained molecules,[29] and therefore the material exhibits a lower driving force to reduce intramolecular strain, because of the lack of connectivity between high- and low-strained regions of a molecule. Hence, aged samples offer higher resistance to indentation penetration at constant force, because of weak intramolecular tension and consequent low molecular displacement (see Fig. 6), which is revealed by lower creep. Longer aging times causes lower creep, because the molecular weight reduction due to aging leads to lower intramolecular tension and therefore to a lower driving force for creep.

The linear correlation between molecular weight and maximum normalized indentation depth for 95°C aging shown in Fig. 5b indicates that chemical aging is the main aging mechanism in this temperature regime. Physical aging plays a minor role for 95°C-aged samples according the first heating of DSC (Fig. 2b). Also, the aging affects the middle and the edge of the sample in the same way. For samples aged with 85°C (Fig. 5a), the edge results lead to linear correlation between the molecular weight and the maximum normalized indentation depth in the double logarithmic presentation. The creep results from the position middle seem to stagnate for longer aging times. Chemical aging of PET is caused by hydrolysis,[29] which means that reactions occur of the ester linkages and the water molecules. We assume that this mechanism happens primarily at the edge of the PET sample, because the crystalline part of PET is impermeable to water, and hydrolysis occurs in the amorphous phase of PET,[29,30] which corresponds to the edge of the sample. The samples aged at 95°C show more signs of physical aging than the 85°C-aged samples, which means that reorientation and recrystallization took place, and that the amorphous and crystalline phases are more homogeneous and spread all over the sample. Thus, water molecules are able to penetrate the whole sample and hydrolysis can take place in the middle and at the edge of the sample.

CONCLUSION AND OUTLOOK

The aging behavior of thin PET films depends on temperature and humidity levels as well as on the duration of the aging. Here, an unaged PET film

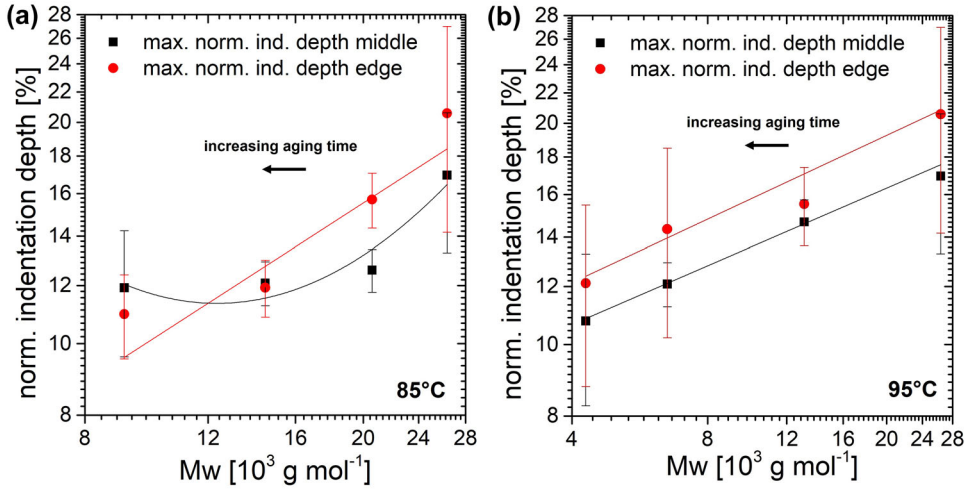

Fig 5. Maximum normalized indentation depth from NI creep tests in the middle of the (a) 85°C and 85% RH and (b) 95°C 85%RH-aged PET samples in comparison with the molecular weight (M_w) at 0 h, 1000 h, 2000 h, and 3000 h aging time in double logarithmic presentation. Black squares indicate the indents obtained from the middle of the sample and red dots the indents from the edge of the sample (Color figure online).

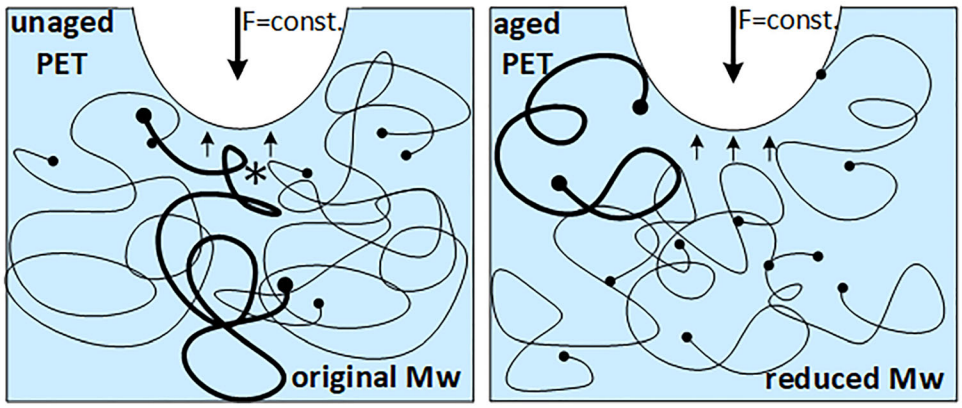

Fig 6. Cross-section of schematic indentation of unaged and aged PET samples by constant force, F: * indicates intramolecular stresses that will lead to more creep of the unaged PET in contrast to the aged PET (adapted from Ref. 40); small arrows indicate pushback forces of the PET.

was investigated to be compared with differently aged PET films in order to detect changes of its mechanical properties.

The main outcome of this investigation is the possibility to determine precise and local elastic moduli of thin PET films with NI comparable to tensile tests. Furthermore, the elastic modulus of highly-embrittled samples can also be determined. NI creep measurements are able to detect degradation with the same sensitivity as GPC measurements in less time. Thus, they provide fast, reliable, and locally resolved information about the early aging of PET.

Future experiments will cover aging behavior of thin films aged by natural weathering as well as by artificial aging. Furthermore, investigations of cross-sections of samples will give more space-resolved information of aging.

ACKNOWLEDGEMENTS

The research work was performed within the COMET-projects “3.S3 Nanoindentation of polymers” and “3.02 PV Casing” at the Polymer Competence Center Leoben GmbH (PCCL, Austria) within the framework of the COMET-program of the Federal Ministry for Transport, Innovation and Technology and the Federal Ministry for Digital and Economic Affairs. The PCCL is funded by the Austrian Government and the State Governments of Styria, Lower Austria and Upper Austria. C.C. acknowledges the support of the Hertha Firnberg Programme by the Austrian Science fund (FWF) (grant no. T 1314-N).

FUNDING

Open access funding provided by Montanuniversität Leoben.

CONFLICT OF INTEREST

On behalf of all authors, the corresponding author states that there is no conflict of interest.

OPEN ACCESS

SUPPLEMENTARY INFORMATION

The online version contains supplementary material available at https://doi.org/10.1007/s11837-022-05278-0.

REFERENCES

1. R. Nisticò, *Polym. Test.* https://doi.org/10.1016/j.polymertesting.2020.106707 (2020).
2. R.P. Borg, O. Baldacchino, and L. Ferrara, *Constr. Build. Mater.* https://doi.org/10.1016/j.conbuildmat.2016.01.029 (2016).
3. G. Oreski and G.M. Wallner, *Sol. Energy*. https://doi.org/10.1016/j.solener.2005.02.008 (2005).
4. A. Omazic, G. Oreski, M. Halwachs, G.C. Eder, C. Hirschl, L. Neumaier, G. Pinter, and M. Erceg, *Sol. Energy Mater. Sol. Cells*. https://doi.org/10.1016/j.solmat.2018.12.027 (2019).
5. W.C. Oliver and G.M. Pharr, *J. Mater. Res.* 7, 1564 (1992).
6. H. Hertz, *Journal für reine und angewandte Mathematik* 92, 156 (1881).
7. V.L. Popov, *Contact Mechanics and Friction* (Springer, Berlin, 2017).
8. P. Christöfl, C. Czibula, M. Berer, G. Oreski, C. Teichert, and G. Pinter, *Polym. Test.* https://doi.org/10.1016/j.polymertesting.2020.106978 (2021).
9. P. Christöfl, C. Czibula, T. Seidlhofer, M. Berer, A. Macher, E. Helfer, T. Schrank, G. Oreski, C. Teichert, and G. Pinter, *Int. J. Polym. Anal. Charact.* https://doi.org/10.1080/1023666X.2021.1968122 (2021).
10. C. Ganser, C. Czibula, D. Tscharnuter, T. Schöberl, C. Teichert, and U. Hirn, *Soft Matter*. https://doi.org/10.1039/C7SM02057K (2018).
11. G.M. Odegard, T.S. Gates, and H.M. Herring, *Exp. Mech.* https://doi.org/10.1007/BF02428185 (2005).
12. S.R. Cohen, and E. Kalfon-Cohen, *Beilstein J. Nanotechnol.* https://doi.org/10.3762/bjnano.4.93 (2013).
13. M.R. VanLandingham, N.K. Chang, P.L. Drzal, C.C. White, and S.H. Chang, *J. Polym. Sci.* 43(14), 1794. (2005).
14. S. Yang and Y. Zhang, *J. Appl. Phys.* https://doi.org/10.1063/1.1651341 (2004).
15. N.S. Allen, M. Edge, M. Mohammadian, and K. Jones, *Polym. Degrad. Stab.* https://doi.org/10.1016/0141-3910(94)90074-4 (2016).
16. K. Looney and B. Brennan, *EU PVSEC*. https://doi.org/10.4229/EUPVSEC20142014-5DO.10.5 (2014).
17. K. Aljoumaa and M. Abboudi, *Appl. Phys.* https://doi.org/10.1007/s00339-015-9518-0 (2016).
18. H. Zhou, E.A. Lofgren, and S.A. Jabarin, *J. Appl. Polym. Sci.* 112(5), 2906 (2009).
19. D.E. Mansour, F. Swientek, I. Kaaya, D. Philipp, and L. Pitta Bauermann, *EU PVSEC*. https://doi.org/10.4229/35thEUPVSEC20182018-5CV.3.28 (2018).
20. B. Ottersböck, G. Oreski, and G. Pinter, *J. Appl. Polym. Sci.* https://doi.org/10.1002/app.44230 (2016).
21. A. Flores, F. Ania, and F.J. Baltà-Calleja, *Polymer*. https://doi.org/10.1016/j.polymer.2008.11.037 (2009).
22. B. Ottersböck, *Natural and artificial weathering tests of polymer films used in solar applications* (Doctoral dissertation, Montanuniversität Leoben, Leoben, Austria, 2017).
23. J. Woirgard, J.C. Dargenton, C. Tromas, and V. Audurier, *Surf. Coat. Technol.* 100–101, 103. (1998).
24. X.D. Hou and N.M. Jennett, *Polym. Test.* 70, 297 (2018).
25. S.L. Zhang and J.C.M. Li, *J. Polym. Sci.-Part B*. https://doi.org/10.1002/polb.10542 (2004).
26. International Organisation for Standardisation, ISO 527-3. 1995. Plastics - Determination of tensile properties: Part 3: Test conditions for films and sheets, 527-3.
27. K. Weisskopf, *J. Polym. Sci.* 26, 1919 (1988).
28. International Organisation for Standardisation, ISO 11357-3. 1999. Plastics – Differential scanning calorimetry (DSC) Part 3: Determination of temperature and enthalpy of melting and crystallization, 11357-3.
29. G.W. Ehrenstein and S. Pongratz, *Beständigkeit von Kunststoffen* (Carl Hanser Verlag, Munich, 2007).
30. S.S. Hosseini, S. Taheri, A. Zadhoush, and A. Mehrabani-Zeinabad, *J. Appl. Polym. Sci.* 103(4), 2304 (2007).
31. M. Edge, M. Hayes, M. Mohammadian, N.S. Allen, T.S. Jewitt, K. Brems, and K. Jones, *Polym. Degrad. Stab.* 32(2), 131 (1991).
32. H. Hagihara, A. Oishi, M. Funabashi, M. Kunioka, and H. Suda, *Polym. Degrad. Stab.* 110, 389 (2014).
33. L.C.E. Struick, *Polym. Eng. Sci.* 17, 3 (1977).
34. B. Fayolle, E. Richaud, and X. Colin, *J. Mater. Sci.* 43, 6999 (2008).
35. A. Flores and F.J. Baltá-Calleja, *Philos. Mag. A*. https://doi.org/10.1080/01418619808239987 (1998).
36. T. Pertin, G. Minatchy, M. Adoue, A. Flory, and L. Romana, *Polym. Test.* https://doi.org/10.1016/j.polymertesting.2019.106194 (2020).
37. C. Andreia, J.V. Tavares, C.M. Gulminea, and L.A. Lepienski, *Polym. Degrad. Stab.* https://doi.org/10.1016/S0141-3910(03)00108-3 (2003).
38. A. Flores and F.J. Baltà-Calleja, *J. Appl. Phys.* https://doi.org/10.1063/1.1418000 (2001).
39. D.C. Miller, M. Owen-Bellini, and P.L. Hacke, *Sol. Energy Mater. Sol. Cells*. https://doi.org/10.1016/j.solmat.2019.110082 (2016).
40. C. Tweedie and K. Van Vliet, *J. Mater. Res.* https://doi.org/10.1557/jmr.2006.0197 (2006).